Coexistence of Superconductivity and Ferromagnetism in Two Dimensions

D. A. Dikin,[1] M. Mehta,[1] C. W. Bark,[2] C. M. Folkman,[2] C. B. Eom,[2] and V. Chandrasekhar[1,*]

[1]*Department of Physics and Astronomy, Northwestern University, Evanston, Illinois 60208, USA*
[2]*Department of Materials Science and Engineering, University of Wisconsin-Madison, Madison, Wisconsin 53706, USA*
(Received 18 March 2011; published 25 July 2011)

Ferromagnetism is usually considered to be incompatible with conventional superconductivity, as it destroys the singlet correlations responsible for the pairing interaction. Superconductivity and ferromagnetism are known to coexist in only a few bulk rare-earth materials. Here we report evidence for their coexistence in a two-dimensional system: the interface between two bulk insulators, $LaAlO_3$ (LAO) and $SrTiO_3$ (STO), a system that has been studied intensively recently. Magnetoresistance, Hall, and electric-field dependence measurements suggest that there are two distinct bands of charge carriers that contribute to the interface conductivity. The sensitivity of properties of the interface to an electric field makes this a fascinating system for the study of the interplay between superconductivity and magnetism.

There has been much interest recently in the conducting interface that forms between the two band insulators, $SrTiO_3$ (STO) and $LaAlO_3$ (LAO) [1–13]. This interface shows a rich variety of behavior, including superconductivity [3,9,10], magnetism [4,8,11,13], and electric-field controlled metal-insulator [2,6] and superconductor-insulator transitions [7,9]. Two important mechanisms have been proposed for the creation of the conducting layer at the interface [5,8,14–17]: (i) charge transfer from the LAO to the Ti^{+2} ions at the interface (the so-called polar catastrophe mechanism) and (ii) conduction due to oxygen vacancies, which can be controlled by growth or post-growth annealing conditions. The Ti bands are also thought to contribute to the magnetism seen in some samples [14].

The electronic characteristics are very sensitive to the growth conditions: generally, it is found that samples grown in an environment with low oxygen partial pressure P_{O_2} have more oxygen vacancies and are consequently more conducting; the conductivity is reduced if the samples are grown in high P_{O_2}, or subjected to a post-growth oxygen anneal [8,13]. It is not only the conductivity that is sensitive to growth conditions: superconductivity is observed in samples grown in intermediate P_{O_2} [8], and signatures of ferromagnetism are observed for samples grown in high P_{O_2} [4,13], although both phenomena have not been observed until now in the same sample. Here we report measurements on LAO/STO interface structures where both phases are seen simultaneously at low temperatures. Magnetoresistance and Hall measurements indicate that there are at least two bands of charge carriers in the system. Earlier theoretical calculations [18] have pointed to a ferromagnetic ground state of the system due to the multivalent nature of the Ti ions at the interface, but the origin of superconductivity is still not clear. This system joins only a few other bulk materials in which superconductivity and ferromagnetism have been observed simultaneously [19–22], with two critical

differences: both the superconductivity and the magnetism are confined to a two-dimensional interface, and the electronic properties of this interface can be tuned over a wide range by means of an electric field. Consequently, it forms a unique system for the investigation of the interplay between superconductivity and magnetism.

The films in this work had 10 unit cells (uc) of LAO grown by pulsed laser deposition at $P_{O_2} = 10^{-3}$ mbar on TiO_2 terminated (001) STO single crystal substrates [23]. For electrical measurements, a Hall bar geometry was patterned by photolithography and etched using argon ion milling that removed the LAO layers and a few layers of STO. Measurements confirmed that the bare etched STO was not conducting from room temperature down to milli-kelvin temperatures. A gate voltage V_g applied to the back of the substrate was used to modulate the conductance of the devices. While the qualitative behavior of all the samples was the same, the devices showed small sample-to-sample variations that were only evident at millikelvin temperatures. The origin of these variations is not clear at the moment. We shall concentrate in this Letter on data from a single longitudinal section and its adjacent Hall configurations that showed the sharpest superconducting transitions.

The normal state and superconducting characteristics and their dependence on V_g and temperature T are similar to that seen by other groups [3,7,9] [Fig. 1(a)]. The current-voltage curves also show a characteristic superconducting signature with a critical current I_c that vanishes when $V_g < -20$ V [Fig. 1(b)]. However, I_c and the transition temperature T_c do not increase monotonically with increasing V_g, but show maxima at $V_g \simeq 80$ V [Fig. 1(c)].

Figure 2(a) shows the superconducting transition at $V_g = 80$ V at a few different values of magnetic field H applied perpendicular to the film plane. Defining T_c as the temperature corresponding to half the normal state resistance, a plot of $T_c(H)$ is shown as an inset to the figure.
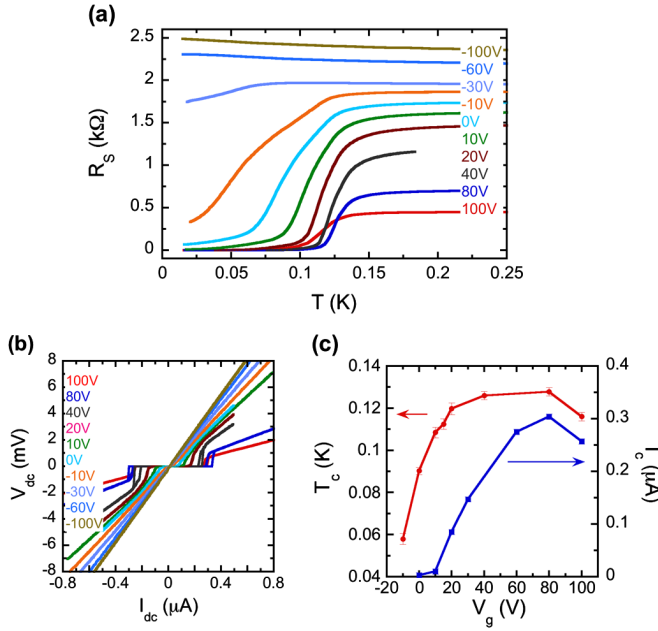
FIG. 1 (color online).   (a) Superconducting transition at differ-ent gate voltages V_g. (b) Current-voltage characteristics of the sample at 15 mK. (c) Transition temperature T_c (defined as the midpoint of the resistive transition) and critical current (defined as the current at which the sample switches to the resistive state on ramping the current up from zero) as a function of V_g. Both measures indicate that the maximal superconducting properties are obtained for $V_g \simeq 80$ V. Error bars indicate the difference in T_c measured between cooling and warming traces.

For two-dimensional superconductors in this field orienta-tion, $T_c(H)$ should be linear, its slope proportional to the Ginzburg-Landau coherence length ξ_0 [24]. A linear fit gives $\xi_0 = 64$ nm, close to that reported previously [3,10].

However, this method of determining $T_c(H)$ misses some of the more novel and interesting behavior of this system. To show this behavior, we map $T_c(H)$ continuously by controlling the sample temperature so that the sample resistance R_S remains fixed as we ramp the magnetic field. Figure 2(b) shows $T_c(H)$ for three different resistance bias points at $V_g = 80$ V. The most striking aspect of the data is that the behavior is hysteretic as a function of H. Consider the curve corresponding to the bias point $R_S = 208$ Ω, slightly lower than the midpoint of the transition. Increasing the magnetic field from negative values towards $H = 0$, T_c shows a smooth increase that is almost linear. The slope of this linear curve gives $\xi_0 = 71$ nm, close to the value obtained from Fig. 2(a). On ramping H beyond zero, however, the behavior becomes nonmonotonic: in particular, there is a local minimum at $H \simeq 7$ mT. Increasing H further, $T_c(H)$ becomes monotonic again. Reversing the ramp direction results in a mirror image of the first trace, giving rise to a characteristic "butterfly" curve. Similar behavior is seen at other gate voltages for which the sample goes superconducting [Fig. 2(c)].
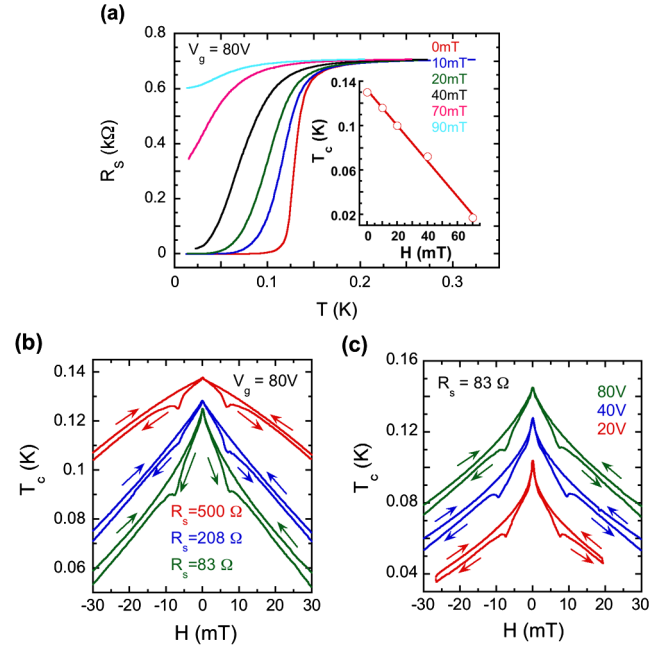
FIG. 2 (color online).   (a) Superconducting transition for $V_g = 80$ V, at a few different magnetic fields. Inset: T_c vs H obtained from these data. T_c is defined by the midpoint of the resistive transition. The line represents a linear fit to the data points, with a slope of 1.6 mK/mT, giving a zero temperature coherence length of $\xi_0 = 64$ nm. (b) Phase diagram, T_c vs H, for a gate voltage of $V_g = 80$ V, where the superconducting properties are maximal. The three curves represent different resistance bias points along the superconducting transition, with the normal state resistance per square being 704 Ω. The arrows mark the direction of the magnetic field ramp. (c) Phase diagrams at a bias point of $R_S = 83$ Ω, at the foot of the resistive transition, at three different gate voltages. Data for $V_g = 40$ V are shifted by 10 mK and data for $V_g = 80$ V by 20 mK for clarity.

Hysteretic behavior and butterfly curves in the magnetic field dependence of electrical characteristics are signatures of underlying ferromagnetic order in a sample. Such be-havior has already been reported in LAO/STO interface samples: Brinkman et al. [4] demonstrated that hysteretic behavior is observed at low temperatures in 26 uc thick LAO films grown under high P_{O_2}; more recently, Ariando et al. [13] were able to observe hysteretic magnetization curves coexisting with paramagnetic and diamagnetic be-havior in samples also grown in high P_{O_2} that persisted to room temperature. For low P_{O_2} during growth, Huijben et al. [8] note that a low sheet resistance and metallic behavior are observed; for intermediate P_{O_2}, the samples go superconducting; while for high P_{O_2} magnetic behavior is seen. These experiments suggest to us that the magne-tism is associated with the polar catastrophe mechanism, while the superconductivity is associated with the presence of oxygen vacancies. However, in all previous experiments, the magnetic and superconducting regimes were quite dis-tinct. In contrast, our samples, which are grown under high

P_{O_2} and have R_S consistent with the superconducting samples measured by others [8], show a coexistence of superconductivity and ferromagnetism. The electronic properties of LAO/STO interfaces are extremely sensitive to growth conditions: samples grown by different groups with nominally identical growth conditions show some variations in electronic properties. Our samples appear to be in a growth regime where both phenomena coexist.

Caviglia *et al.* [12] have reported weak (anti)localization magnetoresistance (MR) in LAO/STO samples. At first sight, the data from our samples appear to be very similar to their data. Figure 3(a) shows the MR of the sample at a few different temperatures at $V_g = -100$ V, not in the superconducting regime. The magnitude of the resistance change and the sharpness of the resistance dip near zero field increase with decreasing temperature, consistent with
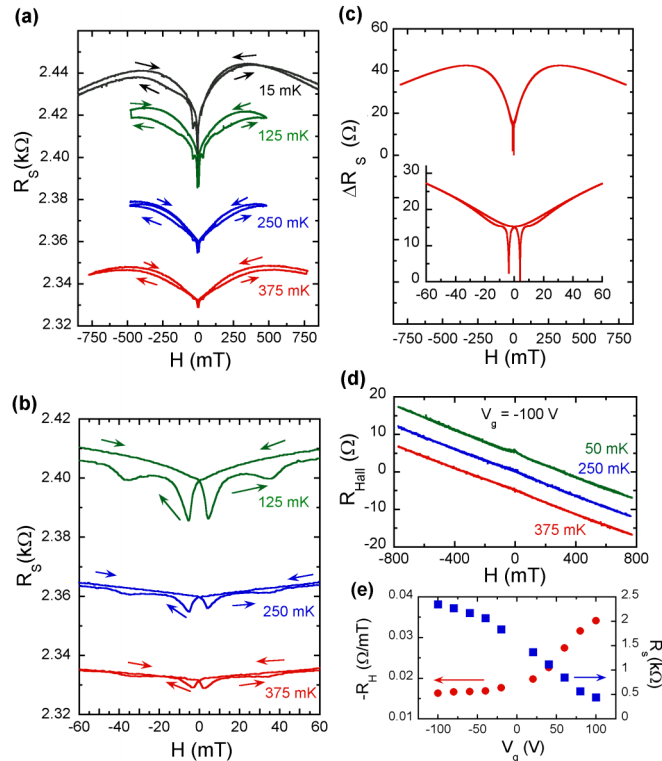

FIG. 3 (color online). (a) Magnetoresistance (MR) at $V_g = -100$ V at four different temperatures. (b) Expansion of the low-field data of (a) for the three highest temperatures. (c) Simulation of the longitudinal MR assuming weak localization contributions from two parallel conducting channels. The inset shows an expanded view of the zero field region, showing the hysteresis and the nonmonotonic dependence seen in the experimental data. (d) Hall resistance at $V_g = -100$ V at three different temperatures. Data for 50 mK and 375 mK have been offset by $+5$ and -5 Ω, respectively. (e) Hall coefficient and zero field longitudinal resistance at different gate voltages at 270 mK. The longitudinal resistance decreases with increasing gate voltage, but the Hall coefficient, nominally inversely proportional to the electron density, increases.

a phase coherence length that increases with decreasing temperature. However, a closer look at the low-field MR, shown in Fig. 3(b), reveals some significant differences from [12]. In addition to the nonmonotonic MR over a large field scale [Fig. 3(a)], the samples show an additional resistance dip near zero field whose magnitude increases and width decreases with decreasing temperature. This behavior, which is characteristic of weak localization (WL) [25], suggests that there are two independent carrier gases that contribute to the conductance of the device in parallel, each with its own WL contribution. The MR also shows a hysteretic butterfly pattern similar to that seen in $T_c(H)$ [Figs. 2(b) and 2(c)], indicating that local magnetic fields arising from magnetic order also modulate quantum interference in the carrier gases.

To demonstrate the feasibility of this picture, we have simulated the WL contribution of two parallel two-dimensional gases in the presence of an external magnetic field and a magnetic field arising from a hysteretic intrinsic magnetization. To calculate the WL contribution in the presence of spin-orbit scattering, we use the formalism of Santhanam *et al.* [26]. The resulting curve is shown in Fig. 3(c). The simulation qualitatively reproduces the experimental features: a nonmonotonic MR over a large field scale, and a smaller nonmonotonic MR over a smaller field scale, with hysteresis due to intrinsic magnetic order. In the simulation, the larger contribution (88%) is due to a carrier gas that has short phase coherence (L_ϕ) and spin-orbit scattering (L_{so}) lengths ($L_\phi = 0.17$ μm, $L_{so} = 0.03$ μm), while the remaining contribution is due to a carrier gas with longer L_ϕ and L_{so} ($L_\phi = 4.5$ μm, $L_{so} = 0.45$ μm). Experimentally, we observe an increase in the amplitude of the low-field MR as the sample approaches the superconducting transition (by changing V_g, for example), which is probably due to the contribution of Maki-Thompson superconducting fluctuations [27] whose MR field scale is determined by L_ϕ [26], and which is expected to increase exponentially as $T \to T_c$.

Further evidence for two parallel conduction channels can be seen in the Hall resistance data. Figure 3(d) shows the Hall resistance R_{Hall} of the sample at $V_g = -100$ V at three different temperatures. The sign of the slope of $R_{Hall}(H)$, R_H, corresponds to negatively charged carriers with a density $n \simeq 4.4 \times 10^{13}/cm^2$, assuming a single carrier band. If there were only one electron gas at the interface, increasing V_g should increase n, decreasing both R_S and R_H. As shown in Fig. 3(e), increasing V_g does indeed decrease R_S, but *increases* R_H. This behavior is only possible if there are at least two types of carriers involved in electrical transport, with different dependences of densities and mobilities on gate voltage. Evidence for multiple charge carriers has also been observed by other groups [16,17].

For conventional itinerant ferromagnets, it is well known that a finite magnetization should manifest itself as a
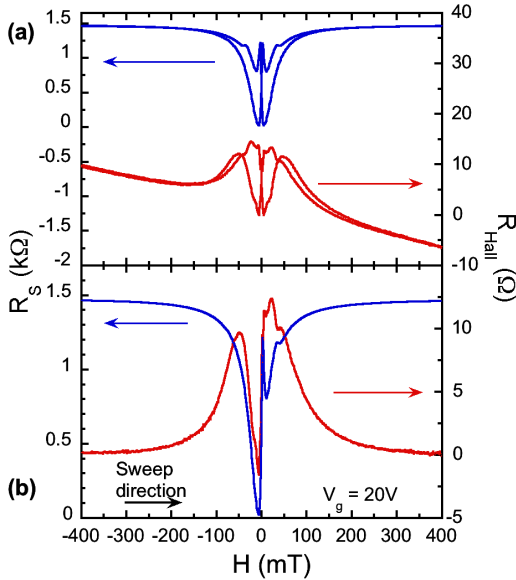
FIG. 4 (color online). (a) Magnetoresistance (top curve) and Hall resistance (bottom curve) at $V_g = 20$ V at 50 mK. (b) Same data as in (a), for one direction of the magnetic field sweep, except the background linear component is subtracted from the Hall resistance.

contribution to R_{Hall} through the anomalous Hall effect [28]. Figure 4(a) shows the longitudinal and Hall MR at $V_g = 20$ V and 50 mK, where $R_S = 0$ when $H = 0$ [Fig. 1(a)]. Figure 4(b) shows the same data with the field sweep in one direction. Here a linear contribution determined by fitting $R_{\mathrm{Hall}}(H)$ at high magnetic fields has been subtracted. It can be seen that some of the structure in $R_S(H)$ also has corresponding signatures in $R_{\mathrm{Hall}}(H)$ (this structure is not due to misalignment of the Hall contacts, which is very small). The structure in $R_S(H)$ and $R_{\mathrm{Hall}}(H)$ for $H > 0$ (for this field sweep direction) is also seen at other gate voltages, further from the superconducting transition. We believe that this structure in the Hall resistance is due to an anomalous Hall effect arising from the interaction of the charge carriers with the magnetic moments at the interface, but the structure seen in Fig. 4(b) indicates that this interaction is more complicated than that in simple itinerant ferromagnets, and warrants further investigation. The features in $R_{\mathrm{Hall}}(H)$ change with V_g. The sharp dip in both the longitudinal and the Hall resistance for $H < 0$ appears only close to the superconducting transition, and may be associated with vortex flow in the superconductor [29].

In summary, the interface between LAO and STO shows a rich variety of behavior, including interacting ferromagnetism and superconductivity. Our measurements indicate that there are two different types of charge carriers in the system. The ability to tune the properties of the system by means of a gate voltage makes this a fascinating system for studying competing cooperative phenomena in two dimensions.

*v-chandrasekhar@northwestern.edu
[1] A. Ohtomo and H. Y. Hwang, Nature (London) **427**, 423 (2004).
[2] S. Thiel, G. Hammerl, A. Schmehl, C. W. Schneider, and J. Mannhart, Science **313**, 1942 (2006).
[3] N. Reyren et al., Science **317**, 1196 (2007).
[4] A. Brinkman et al., Nature Mater. **6**, 493 (2007).
[5] W. Siemons et al., Phys. Rev. Lett. **98**, 196802 (2007).
[6] C. Cen et al., Nature Mater. **7**, 298 (2008).
[7] T. Schneider, A. D. Caviglia, S. Gariglio, N. Reyren, and J.-M. Triscone, Phys. Rev. B **79**, 184502 (2009).
[8] M. Huijben et al., Adv. Mater. **21**, 1665 (2009).
[9] A. D. Caviglia et al., Nature (London) **456**, 624 (2008).
[10] M. Ben Shalom, M. Sachs, D. Rakhmilevitch, A. Palevski, and Y. Dagan, Phys. Rev. Lett. **104**, 126802 (2010).
[11] S. Seri and L. Klein, Phys. Rev. B **80**, 180410(R) (2009).
[12] A. D. Caviglia et al., Phys. Rev. Lett. **104**, 126803 (2010).
[13] Ariando et al., Nature Commun. **2**, 188 (2011).
[14] For a review, see H. Chen, A. M. Kolpak, and S. Ismail-Beigi, Adv. Mater. **22**, 2881 (2010).
[15] A. Kalabukhov et al., Phys. Rev. B **75**, 121404(R) (2007).
[16] S. S. A. Seo et al., Appl. Phys. Lett. **95**, 082 107 (2009).
[17] T. Fix, F. Schoofs, J. L. MacManus-Driscoll, and M. G. Blamire, Phys. Rev. Lett. **103**, 166802 (2009).
[18] R. Pentcheva and W. E. Pickett, Phys. Rev. B **74**, 035112 (2006).
[19] I. Felner, U. Asaf, Y. Levi, and O. Millo, Phys. Rev. B **55**, R3374 (1997).
[20] S. S. Saxena et al., Nature (London) **406**, 587 (2000).
[21] D. Aoki et al., Nature (London) **413**, 613 (2001).
[22] C. Pfleiderer et al., Nature (London) **412**, 58 (2001).
[23] Film synthesis details are similar to those described in J. W. Park et al., Nature Commun. **1**, 94 (2010); C. W. Bark et al., Proc. Natl. Acad. Sci. U.S.A. **108**, 4720 (2011).
[24] J. B. Ketterson and S. N. Song, Superconductivity (Cambridge University Press, Cambridge, England, 2000).
[25] G. Bergmann, Phys. Rep. **107**, 1 (1984).
[26] P. Santhanam, S. Wind, and D. E. Prober, Phys. Rev. B **35**, 3188 (1987). We do not take into account the contribution due to Maki-Thompson fluctuations [27], since we are far from the superconducting transition at $V_g = -100$ V.
[27] K. Maki, Prog. Theor. Phys. **39**, 897 (1968); R. S. Thompson, Phys. Rev. B **1**, 327 (1970).
[28] N. Nagaosa, J. Sinova, S. Onada, A. H. MacDonald, and N. P. Ong, Rev. Mod. Phys. **82**, 1539 (2010).
[29] S. J. Hagen, C. J. Lobb, R. L. Greene, M. G. Forrester, and J. H. Kang, Phys. Rev. B **41**, 11 630 (1990).